_____

FLUTTER ANALYSIS OF BRIDGE DECKS USING LATTICE BOLTZMANN METHOD

L. Ketong* – T. Aiping – L. Yuejun – Z. Hao

School of Civil Engineering, Harbin Institute of Technology, Harbin, Hei Longjiang Province, China

ARTICLE INFO	Abstract:
	Aiming at using the Lattice Boltzmann Method for flutter analysis of the bridge decks, a fluid-structure interaction algorithm is developed within the framework of multiple –relaxation- time Lattice Boltzmann Method. In the present algorithm, the unsteady fluid dynamics is computed by the extended two-dimensional Lattice Boltzmann Method by incorporating the dynamic Smagorinsky subgrid scale model, while the structure is modelled by an elastically suspended rigid body and its dynamic analysis is performed by using a Runge–Kutta method. A staggered coupling strategy is adopted to couple the fluid solver and the structure solver. To demonstrate the applicability of the presented algorithm, flutter analyses of the Second Forth Road Bridge and the Guamá River Bridge are employed. The numerical results are compared with wind tunnel measurements. It is shown that the presented algorithm has a good prediction for the flutter onset velocities of the Forth Road Bridge and the Guamá River Bridge and thus indicates, to a certain extent, the applicability of the presented algorithm.

1. Introduction

The modern long-span bridges have become more flexible and slender, and thus more susceptible to a variety of wind-induced vibrations. Among all wind-induced structural vibrations, flutter is one of the most important aerodynamic instabilities observed in bridge structures, as it may result in catastrophic structural failure [1]. Therefore, flutter instability is a major concern in the design of modern long-span bridges.

Flutter analysis was first treated by means of experimental studies using boundary layer wind tunnels. Recently, with advances and improvements in computational power and the area of computational fluid dynamics (CFD), numerical simulation has become a very attractive way to investigate bridge aeroelastic instability, and several computational fluid dynamics (CFD) algorithms have been developed to address these needs. Robertson et al. [2] used a 2D hp/Spectral fluid

_____

* Corresponding author. Tel.: 8615945688291
Email address: ketong_1982@163.com

solver to investigate the fluid-structure interaction (FSI) of a bridge deck in a cross wind. The study has shown a detailed investigation on prediction techniques of the flutter onset velocity using the free oscillation simulations and the analytical, semi-analytical methods, respectively. The predicted flutter onset velocity was found to be in good agreement with the experimental results. Frandsen [3] approached the fluid-structure interaction problems using a finite element procedure to predict the aeroelastic behavior of long-span bridges. Despite a laminar flow assumption, the finite element procedure predicted that a flutter onset velocity will be in good agreement with wind tunnel experiments. Badia and Codina [4] presented a fluid-structure iterative algorithm using pressure segregation methods. They reported that the method showed good convergence behaviour for aeroelastic simulation of the bridges. However, the computed flutter onset velocity of 55 m/s was vastly underestimated compared with the 65–70 m/s obtained from wind tunnel tests. Braun et al. [5] employed an explicit two-step Taylor-Galerkin method with an Arbitrary Lagrangean-Eulerian description for solving the flow around oscillating bridge sections to predict the flutter critical velocity. The simulated results compared well with the experimental results. Sarkic et al. [6] applied two dimensional (2D) Unsteady Reynolds-Averaged Navier–Stokes method with $k-\omega$ SST turbulence model to numerical simulations of the static forces and flutter derivatives for asymmetric bridge deck section. A similar numerical approach was also employed by Miranda et al. [7] and Brusiani et al. [8] to perform the aerodynamic analysis of the bridge. Recently, Farsani et al. [9] utilized the grid free discrete vortex method for determining the flutter characteristics of a box girder section. Other researchers, such as Selvam et al. [10, 11], Sarwar et al. [12] and Mannini et al. [13], also paid much attention to this subject. Many existing fluid-structure interaction algorithms are developed based on the finite volume method and finite element method. Although these algorithms can be employed to simulate wind-structure interaction problems, they may not be computationally effective when the large movements of the structure are present due to intensive computations involved in the continuous generation of new meshes to circumvent severe mesh distortion near the fluid-structure interface.

In recent years, the Lattice Boltzmann Method (LBM) [14, 15], as an accurate and efficient numerical approach, has gained a fame amongst the community of computational fluid dynamics. Compared with traditional computational fluid dynamics methods (for instance, finite volume method and finite element method), Lattice Boltzmann Method has many distinct advantages, such as simplicity of programming, favorable parallel-computing structure and capability in dealing with complex geometries. Especially the use of an Eulerian grid to represent the flow field makes Lattice Boltzmann Method an ideal numerical tool for avoiding mesh distortion inherent in various finite element or finite volume-based techniques for fluid-structure interaction simulation. Substantial efforts have been devoted to fluid-structure interaction based on Lattice Boltzmann Method. Garcia et al. [16] presented a method for the fluid-structure interaction by a hybrid approach that uses Lattice Boltzmann Method for the fluid dynamics analysis and fixed-grid finite element method for the structural analysis. De Rosis et al. [17] investigated the interaction of fluid flow with flexibly supported rigid body. In their algorithm, fluid dynamics was computed by Lattice Boltzmann Method, while the structure dynamic analysis was performed using the Time Discontinuous Galerkin (TDG) method. More recently the authors developed a acoupled lattice Boltzmann-finite element approach with the immersed boundary method to implement aeroelastic study of flexible flapping wings [18]. In addition, an arbitrary Lagrangian–Eulerian approach for the simulation of immersed moving solids with the BGK-Lattice Boltzmann Method was proposed in [19]. However, these methods cannot be used for wind-structure interaction simulation. Because the wind fields are typical high Reynolds flows while Lattice Boltzmann Method is developed for laminar flows at low Reynolds numbers.

The objective of this work is to investigate the use of Lattice Boltzmann Method to predict the flutter onset velocity of the bridge. In this paper, a fluid-structure interaction algorithm will be developed based on the extended multiple – relaxation - time Lattice Boltzmann Method (MRT-LBM) [20]. Fluid-structure interaction is considered as a rigid body mounted on the wind fields with elastic restrains. The unsteady wind field past the bridge decks at high Reynolds number is solved by large

_____

eddy simulation within the framework of multiple-relaxation- time Lattice Boltzmann Method on a fixed grid. The structure can move on the grid and its dynamic analysis is accomplished using Runge–Kutta method. The coupling between fluid and structure is performed applying the interpolated bounce-back (IBB) scheme [21] and a refill procedure at the interface. In order to validate the present computational scheme, we apply it to flutter analysis of the Second Forth Road Bridge and the Guama River Bridge.

2. Numerical methods

2.1 Fluid solver

2.1.1 MRT-LBM

Among various Lattice Boltzmann Methods, the LBGK-Lattice Boltzmann Method is the most widely used one due to its simplicity. However, the numerical instability may appear in the LBGK-Lattice Boltzmann Method because it uses single relaxation time collision operator [22]. The deficiency in this method can be overcome with the use of the Lattice Boltzmann model using multiple relaxation time collision operator [20], and therefore, we use the multiple relaxation time Lattice Boltzmann Method to simulate the high Reynolds number flows past the bridge decks .

The Lattice Boltzmann Method views fluids as a group of discrete particles residing on a discrete lattice. The description of these particles is made by a particle distribution function $f_k(x,t)$, which indicates the particle amount moving with the *i*th lattice velocity $\mathbf{c}_k$ at position x and time t . In multiple – relaxation - time Lattice Boltzmann Method, the equation for the time evolution of f_k is [23]:

$$\mathbf{f}\left(x+\mathbf{c}_k\Delta t,t+\Delta t\right)-\mathbf{f}\left(x,t\right)= \\ -\mathbf{M}^{-1}\mathbf{S}\mathbf{M}\left[\mathbf{f}\left(x,t\right)-\mathbf{f}^{eq}\left(x,t\right)\right], \quad (1)$$

where, $\mathbf{f}^{eq}(x,t)$ is the equilibrium distribution function of $\mathbf{f}(x,t)$, Δt is the time step, $\mathbf{M}$ is the transformation matrix, $\mathbf{S}$ is a diagonal relaxation matrix.

For simulating two-dimensional incompressible flows, the two-dimensional nine-velocity lattice model (D2Q9) (see Fig. 1) is used to recover the Navier–Stokes equations at the macroscopic level. For the D2Q9 model, the discrete velocity set is given as:

$$\mathbf{c}_k = \begin{cases} (0,0), k=0; \\ \left(\cos\left[(k-1)\pi/2\right],\sin\left[(k-1)\pi/2\right]\right)c, k=1,2,3,4, \\ \left(\cos\left[(2k-9)\pi/4\right],\sin\left[(2k-9)\pi/4\right]\right)\sqrt{2}c, k=5,6,7,8, \end{cases} \quad (2)$$

where, $c=\Delta x/\Delta t$ is the lattice speed and Δx is the lattice spacing.
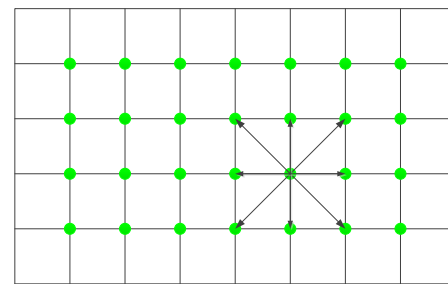
(a) A standard lattice of LBM
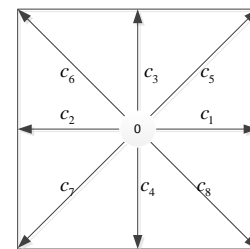
(b) D2Q9 model.

Figure 1. Discretization of LBM and D2Q9 model.

The equilibrium function $\mathbf{f}^{eq}(x,t)$ for each discrete velocity $\mathbf{c}_k$ reads:

$$f_k^{eq} = \rho w_k\left(1+\frac{3}{c^2}\mathbf{c}_k\cdot\mathbf{u}+\frac{9}{2c^4}\left(\mathbf{c}_k\cdot\mathbf{u}\right)^2-\frac{3}{2c^2}\mathbf{u}\cdot\mathbf{u}\right), \\ k=0,1,\cdots,8 \quad (3)$$

where, w_k is the weight coefficient, and given by $w_0=4/9$, $w_{1,2,3,4}=1/9$, and $w_{5,6,7,8}=1/36$. ρ and $\mathbf{u}$

are the macroscopic fluid density and velocity, and can be respectively calculated using:

$$\rho = \sum_{k=0}^{8} f_k, \tag{4}$$

$$\rho\mathbf{u} = \sum_{k=0}^{8} \mathbf{c}_k f_k. \tag{5}$$

The pressure p can be obtained by:

$$p = \rho c_s, \tag{6}$$

where, $c_s = c/\sqrt{3}$ is the sound speed.

In multiple – relaxation - time Lattice Boltzmann Method, the transformation matrix $\mathbf{M}$ transforms $\mathbf{f}(x,t)$ and $\mathbf{f}^{eq}(x,t)$ in the discrete velocity space into the moment space with $\mathbf{m} = \mathbf{M}\mathbf{f}(x,t)$ and $\mathbf{m}^{eq} = \mathbf{M}\mathbf{f}^{eq}(x,t)$, where $\mathbf{m}(x,t)$ is the density distribution function in the moment space. $\mathbf{m}^{eq}(x,t)$ is the equilibrium distribution function of $\mathbf{m}(x,t)$. In D2Q9 model, the distribution functions in moment space are given by:

$$\mathbf{m}(x,t) = \begin{pmatrix} \rho \\ e \\ \varepsilon \\ j_x \\ q_x \\ j_y \\ q_y \\ p_{xx} \\ p_{yy} \end{pmatrix} = \begin{bmatrix} 1 & 1 & 1 & 1 & 1 & 1 & 1 & 1 & 1 \\ -4 & -1 & -1 & -1 & -1 & 2 & 2 & 2 & 2 \\ 4 & -2 & -2 & -2 & -2 & 1 & 1 & 1 & 1 \\ 0 & 1 & 0 & -1 & 0 & 1 & -1 & -1 & -1 \\ 0 & -2 & 0 & 2 & 0 & 1 & -1 & -1 & 1 \\ 0 & 0 & 1 & 0 & -1 & 1 & 1 & -1 & -1 \\ 0 & 0 & -2 & 0 & 2 & 1 & 1 & -1 & -1 \\ 0 & 1 & -1 & 1 & -1 & 0 & 0 & 0 & 0 \\ 0 & 0 & 0 & 0 & 0 & 1 & -1 & 1 & -1 \end{bmatrix} \begin{pmatrix} f_0 \\ f_1 \\ f_2 \\ f_3 \\ f_4 \\ f_5 \\ f_6 \\ f_7 \\ f_8 \end{pmatrix} = \mathbf{M}\mathbf{f}(x,t) \tag{7}$$

$$\mathbf{M} = \begin{bmatrix} 1 & 1 & 1 & 1 & 1 & 1 & 1 & 1 & 1 \\ -4 & -1 & -1 & -1 & -1 & 2 & 2 & 2 & 2 \\ 4 & -2 & -2 & -2 & -2 & 1 & 1 & 1 & 1 \\ 0 & 1 & 0 & -1 & 0 & 1 & -1 & -1 & -1 \\ 0 & -2 & 0 & 2 & 0 & 1 & -1 & -1 & 1 \\ 0 & 0 & 1 & 0 & -1 & 1 & 1 & -1 & -1 \\ 0 & 0 & -2 & 0 & 2 & 1 & 1 & -1 & -1 \\ 0 & 1 & -1 & 1 & -1 & 0 & 0 & 0 & 0 \\ 0 & 0 & 0 & 0 & 0 & 1 & -1 & 1 & -1 \end{bmatrix}, \tag{8}$$

where, ε is related to the square of the energy e, j_x and j_y are the mass flux in two directions, q_x

and q_y correspond to the energy flux in two directions, and p_{xx} and p_{yy} correspond to the diagonal and off-diagonal component of the viscous stress tensor.

The equilibrium distribution functions in moment space are defined as:

$$\mathbf{m}^{eq} = \left(m_0^{eq}, m_1^{eq}, m_2^{eq}, m_3^{eq}, m_4^{eq}, m_5^{eq}, m_6^{eq}, m_7^{eq}, m_8^{eq}\right)^T \tag{9}$$

where, $m_0^{eq} = \rho$, $m_1^{eq} = -2\rho + 3\left(j_x^2 + j_y^2\right)$, $m_2^{eq} = \rho - 3\left(j_x^2 + j_y^2\right)$, $m_3^{eq} = -m_4^{eq} = j_x$, $m_5^{eq} = -m_6^{eq} = j_y$, $m_7^{eq} = j_x^2 - j_y^2$, $m_8^{eq} = j_x j_y$, $j_x = \rho u_x = \sum_i f_i^{eq} c_{ix}$, $j_y = \rho u_y = \sum_i f_i^{eq} c_{iy}$.

The diagonal matrix $\mathbf{S}$ of relaxation rates s_k is given by:

$$\mathbf{S} = diag\left(s_0, s_1, s_2, s_3, s_4, s_5, s_6, s_7, s_8\right). \tag{10}$$

The relaxation rates s_0, s_3 and s_5 are arbitrary, and are set to 0 in the following simulations. The relaxation rate s_1 is related to the bulk viscosity ζ, namely, $\zeta = (1/s_1 - 1/2)/6$. In this study, the relaxation rates $s_1 = s_2 = s_4 = s_6 = 1.1$ are used. s_7 and s_8 are related to kinematic viscosity υ, namely,

$$s_7 = s_8 = 2/(6\upsilon + 1). \tag{11}$$

The evolution process of multiple- relaxation- time Lattice Boltzmann Method consists of two essential steps, i.e., collision and streaming, to reveal the flow phenomena. Unlike the BGK-Lattice Boltzmann Method, the collision sub-step of multiple- relaxation - time Lattice Boltzmann Method is performed in moment space:

$$\overline{f}_k(x,t) = f_k(x,t) - \mathbf{M}^{-1}\mathbf{S}\left(\mathbf{m}(x,t) - \mathbf{m}^{eq}(x,t)\right). \tag{12}$$

The streaming of multiple- relaxation- time Lattice Boltzmann Method is still executed in velocity space

$$f_k(x + \mathbf{c}_k\Delta t, t + \Delta t) = \overline{f}_k(x,t), \tag{13}$$

_____

where, $\overline{f}_k(x,t)$ denotes the post-collision state of the particle distribution function.

2.1.2   MRT-LBM for simulating turbulent flows

The standard Lattice Boltzmann Method is developed for laminar flows at low Reynolds numbers. In order to simulate the turbulent flows past the bridge decks with the Lattice Boltzmann Method, the basic Lattice Boltzmann Method needs to be extended. In this study, large eddy simulation with dynamic Smagorinsky subgrid scale model is used for the turbulence simulation. The main idea of large-eddy simulation is that the large spatial-scale turbulent eddies are directly resolved, while the smaller-scale eddies are modeled by subgrid scale model. The separation of these scales can be achieved by filtering the Lattice Boltzmann governing equations. Following this concept, the filtered multiple relaxation time Lattice Boltzmann equation can be expressed as:

$$\tilde{\mathbf{f}}\left(x+\mathbf{c}_k\Delta t, t+\Delta t\right)-\tilde{\mathbf{f}}\left(x,t\right)= \\ -\mathbf{M}^{-1}\mathbf{S}^*\mathbf{M}\left[\tilde{\mathbf{f}}\left(x,t\right)-\tilde{\mathbf{f}}^{eq}\left(x,t\right)\right]. \quad (14)$$

where, $\tilde{\mathbf{f}}$ and $\tilde{\mathbf{f}}^{eq}$ are the distribution function and the equilibrium distribution function at the resolved scale, respectively. This equation is exactly the same form as the evolution equation of multiple − relaxation - time Lattice Boltzmann Method (Equation (1)), but the particle functions are replaced by their filtered values. In addition, the turbulence eddy viscosity υ_t is introduced to model the unresolved scale motion. Hence, the total viscosity of the fluid equals the sum of the physical viscosity υ and the eddy viscosity υ_t

$$\upsilon_* = \upsilon + \upsilon_t. \quad (15)$$

Accordingly, $\mathbf{S}^*$ in Eq. (1) is given by:

$$\mathbf{S}^* = diag\left(s_0,s_1,s_2,s_3,s_4,s_5,s_6,s_7^*,s_8^*\right), s_7^* = s_8^* = 2/\left(6\upsilon_*+1\right), \quad (16)$$

where, the relaxation rates $s_0,s_1,s_2,s_3,s_4,s_5,s_6$ are the same as values in $\mathbf{S}$.

In the dynamic Smagorinsky subgrid scale model [24], the turbulence eddy viscosity υ_t can be determined as:

$$\upsilon_t = \left(C\Delta\right)^2|\mathbf{S}|, \quad (17)$$

where, C is the model coefficient, Δ represents the lattice spacing, $\mathbf{S}_{ij} = \left(\partial u_i/\partial x_j + \partial u_j/\partial x_i\right)/2$ is the strain rate tensor, $|\mathbf{S}| = \sqrt{2\mathbf{S}_{ij}\mathbf{S}_{ij}}$. In LBM, instead of the standard finite-difference based formulation the strain rate tensor can be computed directly from non-equilibrium moments of the particle distribution function:

$$\overline{\mathbf{S}}_{ij} = \sum_{\alpha}^{8} c_{\alpha i}c_{\alpha j}f_\alpha^{neq} , \ f_\alpha^{neq} = \mathbf{M}^{-1}\left(\mathrm{m}_\alpha\left(\mathbf{x},t\right)-\mathrm{m}_\alpha^{eq}\left(\mathbf{x},t\right)\right). \quad (18)$$

In this paper, the model coefficient is estimated by means of a dynamic procedure proposed by Premnath et al. in [25]. Once the total viscosity has been determined from Equation (16), large eddy simulation with dynamic Smagorinsky subgrid scale model can be performed within the framework of multiple-relaxation-time Lattice Boltzmann method by calculating the relaxation rates s_7^* and s_8^* at each time step.
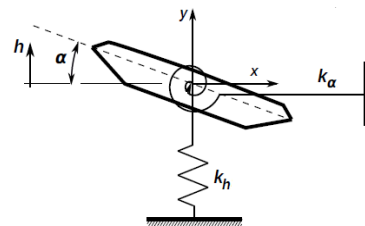
2.2 Structure solver

Figure 2. Two-dimensional rigid body model.

For the numerical aeroelastic analysis of bridges, the 3-dimensional problem is usually reduced to a 2-dimensional problem. In this paper, the structure is modelled using a rigid-body undergoing rotational and vertical motion in wind fields. As shown in Fig. 2, the rigid body is assumed to be mounted on a system composed of elastic springs and dashpots and its equation of motion is expressed by

$$M\ddot{u} + C\dot{u} + Ku = F, \qquad (19)$$

where, $M = diag\left(m, I_\theta\right)$, $C = diag\left(c_h, c_\theta\right)$, $K = diag\left(k_h, k_\theta\right)$; m, I_θ, c_h, c_θ, k_h, k_θ are the system mass, moment of inertia about the elastic axis, structural damping and stiffness in the vertical and rotational directions, respectively; $u = \left(y, \theta\right)^T$ is the displacement vector, y and θ are the vertical displacement and the rotational displacement, respectively; $F = \left(F_y, F_\theta\right)^T$, where $F_y(t)$ and $F_\theta(t)$ indicate the components of the resultant force of the fluid on the structure surface in vertical direction and in rotational direction, their time-dependent schemes are given by

$$F_y(t) = \iint_{\partial\Omega} \sigma n dS, \ F_\theta(t) = \iint_{\partial\Omega} r \times \sigma n dS, \qquad (20)$$

where, σ is the fluid stress tensor, acting upon the boundary $\partial\Omega$ of the structure, n is outer unit normal, and r is the distance from the center of mass.

The above equation is solved explicitly using Runge–Kutta method, which is described by the following set of equations

$$\begin{cases} M\ddot{u}_{t+1} + C\dot{u}_{t+1} + Ku_{t+1} = F_{t+1}, \\ \dot{u}_{t+1} = \dot{u}_t + \dfrac{\Delta t}{6}\left(L + 2P + 2Q + R\right), \\ u_{t+1} = u_t + \Delta t \times \dot{u}_t + \dfrac{\left(\Delta t\right)^2}{6}\left(L + P + Q\right), \end{cases}$$

where L, P, Q, R are given by

$$L = \frac{F(t)}{M} - \frac{C}{M}\dot{u}_t - \frac{K}{M}u_t,$$

$$P = \frac{F(t)}{M} - \frac{C}{M}\left(\dot{u}_t + \frac{\Delta t}{2}L\right) - \frac{K}{M}\left(u_t + \frac{\Delta t}{2}\dot{u}_t\right),$$

$$Q = \frac{F(t)}{M} - \frac{C}{M}\left(\dot{u}_t + \frac{\Delta t}{2}P\right) - \frac{K}{M}\left(u_t + \frac{\Delta t}{2}\dot{u}_t + \frac{\left(\Delta t\right)^2}{4}L\right),$$

$$R = \frac{F(t)}{M} - \frac{C}{M}\left(\dot{u}_t + \Delta t \cdot Q\right) - \frac{K}{M}\left(u_t + \Delta t \cdot \dot{u}_t + \frac{\left(\Delta t\right)^2}{2}P\right).$$

2.3 Fluid-structure coupling

In the present fluid-structure interaction algorithm, the whole computational domain is subdivided by the fixed-grid of Lattice Boltzmann Method and identified as fluid domain and solid domain. The fluid solver is performed on the fluid domain. The position of the structure is continuously updated in the grid with the movement of the fluid-structure interface. As seen in Fig. 3 [17], the fluid and structure solvers are coupled through a staggered coupling strategy.
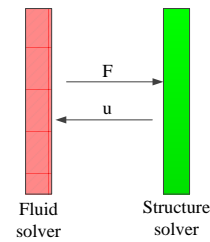

Figure 3. Schematic drawing of the coupling between fluid solver and structure solver [17].

At each time level, large-eddy simulation with dynamic Smagorinsky subgrid scale model is performed within the framework of multiple relaxation-time-Lattice Boltzmann Method to obtain the aerodynamic forces acting on the structure. The aerodynamic forces are then used as an input into the structure solver to predict the displacement of the structure at the next time level. This displacement is then employed to determine the position of the fluid-structure interface in the fluid solver.
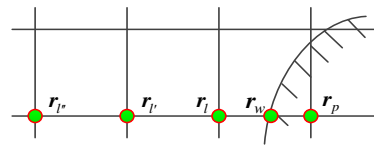

Figure 4. Schematic drawing of IBB scheme.

Lattice nodes adjacent to the solid obstacle do not participate to the standard collision-streaming process of Lattice Boltzmann Method as the immersed body acts as a wall for the motion of particles. In order to achieve the collision-streaming process of Lattice Boltzmann Method and to describe the motion of the structure, the IBB

scheme presented by Yu et al. [21] for tackling moving boundary, is adopted in the current work. As shown in Fig. 4, α is the direction toward the immersed body, $\bar{\alpha}$ denotes the opposite direction of α, $\mathbf{r}_p$ is a solid node, $\mathbf{r}_l, \mathbf{r}_{l'}, \mathbf{r}_{l''}$ are fluid nodes, and $\mathbf{r}_w$ is a boundary node. Due to a lack of information about the neighboring node $\mathbf{r}_p$, the particle distribution function $f_{\bar{\alpha}}(\mathbf{r}_l, t + \Delta t)$ in the $\bar{\alpha}$ - direction away from the solid surface cannot directly obtain from the streaming step of Lattice Boltzmann Method. The IBB scheme established a well-organized interpolation for the unknown distribution. According to the IBB scheme, the particle distribution functions at the solid surface in the α - and $\bar{\alpha}$ - directions can be obtained from the interpolation using the post-collision distribution function $\bar{f}_\alpha(\mathbf{r}_l, t)$ and $\bar{f}_\alpha(\mathbf{r}_{l'}, t)$, and are written as [21]:

$$f_\alpha(\mathbf{r}_w, t+\Delta t) = (1 - \Delta_w)\bar{f}_\alpha(\mathbf{r}_l, t) + \Delta_w \bar{f}_\alpha(\mathbf{r}_{l'}, t), \qquad (21)$$

$$f_{\bar{\alpha}}(\mathbf{r}_w, t+\Delta t) = f_\alpha(\mathbf{r}_w, t+\Delta t) - 2\rho w_\alpha \frac{\mathbf{u}_w \cdot \mathbf{c}_\alpha}{c_s^2}, \qquad (22)$$

respectively, where $\Delta_w = |\mathbf{r}_l - \mathbf{r}_w|/|\mathbf{r}_l - \mathbf{r}_p|$, $\mathbf{u}_w$ is the velocity of the solid surface at the node $\mathbf{r}_w$. Once $f_\alpha(\mathbf{r}_w, t+\Delta t)$ has been computed, $f_{\bar{\alpha}}(\mathbf{r}_l, t+\Delta t)$ can be reconstructed by means of the quadratic interpolation procedure as [21]:

$$f_{\bar{\alpha}}(\mathbf{r}_l, t+\Delta t) = \frac{2}{(1+\Delta_w)(2+\Delta_w)} f_{\bar{\alpha}}(\mathbf{r}_w, t+\Delta t)$$

$$+ \frac{2\Delta_w}{1+\Delta_w} f_{\bar{\alpha}}(\mathbf{r}_{l'}, t+\Delta t) - \frac{\Delta_w}{2+\Delta_w} f_{\bar{\alpha}}(\mathbf{r}_{l''}, t+\Delta t), \qquad (23)$$

Owing to the fixed nature of the grid of Lattice Boltzmann Method, some solid nodes (for example, node A in Fig. 5) enter the fluid domain as a consequence of the movement of the structure and should be activated. Some fluid nodes (for example, node B in Fig. 5) should be simultaneously deactivated since they are covered by the updated structure position [26, 27, 28]. In order to achieve fluid-structure interaction simulations, as illustrated in Fig. 5, a refill procedure is adopted to activate the new fluid node A and to inactivate the solid node B. In the procedure, the node A is activated by

assigning a proper particle distribution function. Specifically, the particle distribution function $f_k(\mathbf{x}_A, t)$ at node A is assigned by operating a linear extrapolation using the particle distribution function at node C and node D, that is,

$$f_k(\mathbf{x}_A, t) = 2f_k(\mathbf{x}_D, t) - f_k(\mathbf{x}_C, t). \qquad (24)$$

For the node B, their particle distribution functions are simply set to zero.
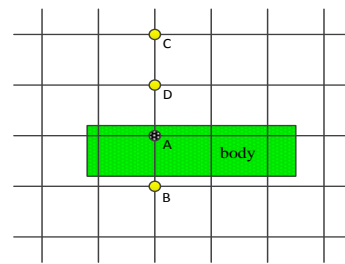
(a) The structure position at time step t
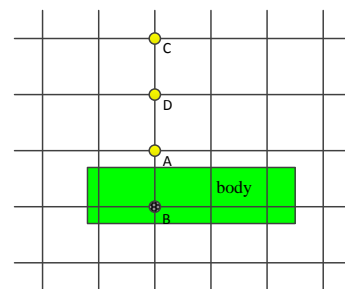
(b) The structure position at time step t+1

Figure 5. Schematic drawing of the refill procedure.

3. Applications for flutter analysis

In order to validate the present computational algorithm, we apply it to flutter analysis of the Second Forth Road Bridge and the Guamá River Bridge in this section. The critical flutter velocity for bridges can be determined using both forced motion and free motion of the bridge cross section in wind tunnel tests. In the forced motion method, the critical flutter velocity is obtained indirectly from the aerodynamic derivatives. While in the free motion method the critical flutter velocity can be observed directly. In the current work, the free vibration method for flutter analysis is carried out in virtual wind tunnel by means of the computational

techniques described above. In virtual wind tunnel, the bridge deck is allowed to oscillate freely in the wind fields under the specified governing structural parameters for various wind velocities. When the translational or rotational amplitude of the oscillations begins to steadily increase or reaches a defined critical displacement, the flutter instability appears, and then the critical velocity can be observed.

3.1 Flutter analysis of the Second Forth Road Bridge

In this section, we present the application of the algorithm described above in flutter analysis of the Second Forth Road Bridge. The flutter behavior of the Second Forth Road Bridge has been previously studied by means of numerical method and wind tunnel tests [2]. We compare our results with the numerical and experimental data in [2]. Fig. 6 shows the bridge cross-section [2]. The structural data used in the analysis are summarized in Table 1 [2].
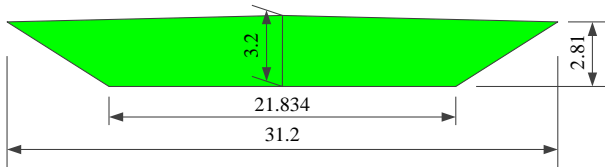

Figure 6. Detail of the Second Forth Road Bridge section.

Table 1. Mechanical properties of the Forth Road Bridge deck

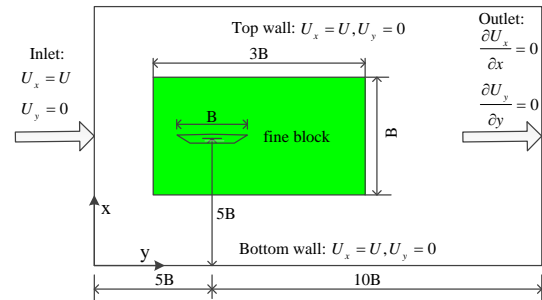| Characteristics	Value
Overall Width (B)	31.2 m
Maximum Depth (D)	3.2 m
Mass per unit length	17300 kg/m
Mass moment of inertia	2130000 kgm^2/m
Vertical natural frequency	0.174 Hz
Angular natural frequency	0.4 Hz
Vertical damping ratio	1.9%
Torsional damping ratio	0.9%

Figure 7. Flow geometry, computational domain and boundary conditions.

The analysis domain is depicted in Fig. 7. In order to eliminate the effect of the boundaries, the elastic centre of the bridge deck is located far enough from the boundaries of the flow field. The elastic centre of the bridge deck is 5B away from the inlet while it is located 4B far from the upper and lower boundaries in our simulation. Turbulence length scales in the vicinity of the immersed body are generally smaller than those at locations far away from the body and therefore require a finer grid to adequately resolve them. Due to a high computational cost associated with the use of such fine grids throughout the computational domain, a multi-block grid refinement scheme, which provides a way to satisfy different resolution requirement in the near wall region and the far field and reduces the memory requirement and computational time, is used in this study. In this method, flow field is divided into blocks. In each block, the grid spacing is uniform with desired resolution. The different grid size blocks are connected only thorough interface. An accurate interface treatment technique between neighboring blocks is adopted in the present study in accordance with Yu et al. [29]. In our simulation, two grid sizes are used with the coarse-to-fine lattice spacing ratio m=$\Delta_c/\Delta_f = 8$ (superscripts c and f are used to represent variables on the coarse and fine blocks, respectively). As illustrated in Fig. 7, the fine-mesh block covers the area from 4B to 7B on x-axis and 4.5B to 5.5B on y-axis, which is about 2% of the whole computational domain by area. There are 307200 fine grids, and 235200 coarse grids with a total of about 542400 grids in the entire domain.

The boundary conditions for the simulations are set as follows. At the inlet, fluid with constant uniform velocity U in x-direction is injected into the domain. The outlet boundary condition is chosen in

_____

such a way that the velocity gradient in the direction normal to the outlet surface is zero. The top and the bottom boundaries are treated as solid walls with the free-slip condition.

The flutter instability of the Second Forth Road Bridge is investigated by analyzing its structural response under wind action with four macroscopic wind velocity levels: 70, 80, 80.05 and 81. The Reynolds number is chosen to be $\mathrm{Re} = UB / \upsilon = 10^5 \sim 10^6$, where U is the inflow velocity and υ is the kinematic viscosity so as to be consistent with the order of the Reynolds number in wind tunnel experiments [2]. Initially, the bridge deck remains fixed with zero angle of attack. After 10000 time steps, the fluid forces acting on the body surface are computed, and then, the bridge deck was allowed to oscillate freely in the wind fields.
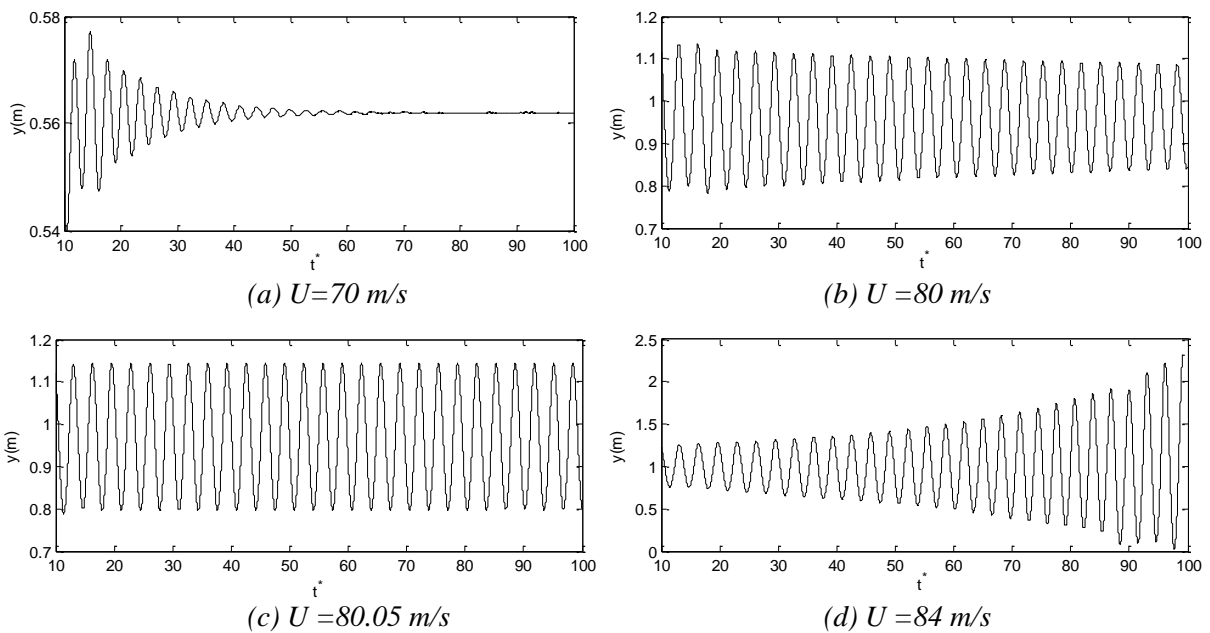

(a) U=70 m/s

(b) U =80 m/s

(c) U =80.05 m/s

(d) U =84 m/s

Figure 8. Vertical displacement of the Second Forth Road Bridge.

(a) U=70 m/s

(b) U =80 m/s

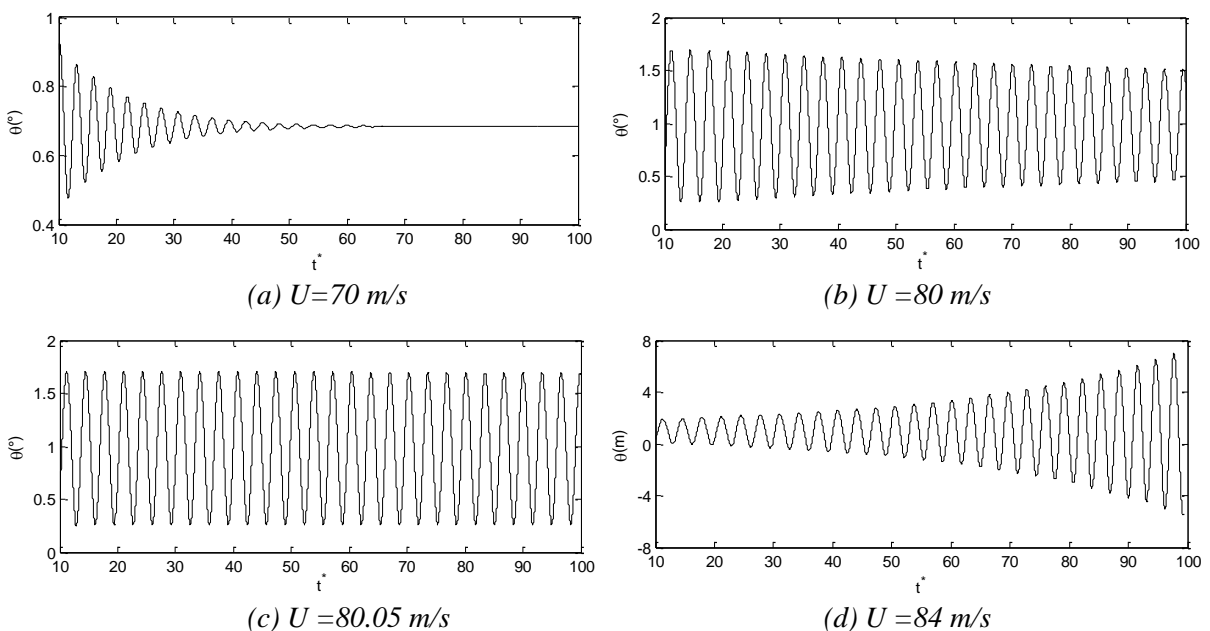*(c) U =80.05 m/s*

(d) U =84 m/s

Figure 9. Rotational displacement of the Second Forth Road Bridge.

Figs. 8 and 9 display the vertical and rotational displacement time histories of the Second Forth Road Bridge for the different velocities, respectively. In Figs. 8 and 9, t^* is the non-dimensionalized time and is defined as $t^* = tU / B$. From Figs. 8 and 9, it can be seen that the vertical and rotational displacement amplitudes grow up as the inflow velocity is increased. For U =70 m/s, the oscillation of the bridge deck quickly decrease for both heave and rotation. At a higher velocity U=80 m/s, the oscillation has a slowly decreasing amplitude of the vertical and rotational displacements because aerodynamic damping, which acts to decrease the structural damping force, gets stronger. The action of structural damping is clearly observed in response to the bridge deck at these two wind velocity levels, where the aerodynamic damping is lower than structural damping and the structure is safe. At the velocity U=80.05 m/s, the oscillations maintain their magnitude. It suggests that aerodynamic damping is equal to structural damping at U=80.05 m/s and U=80.05 m/s is the critical velocity for the onset of flutter instability. In the case of the inflow velocity U=81 m/s, the structural response is characterized by a continuous increase in the amplitude of the vertical and rotational displacements. This reveals that, at U=81 m/s, total damping (structural damping + aerodynamic damping) becomes negative, leading to structural instability. In fact, the instability is vertical and rotational (see Figs. 8 (d) and 9 (d)). From the computed results illustrated in Figs. 8 and 9, it can be found that aerodynamic damping is dependent on the inflow velocity while the structural instability lies in aerodynamic damping. As the inflow velocity is increased, aerodynamic damping gets stronger. When aerodynamic damping is similar or greater than structural damping, the total damping becomes negative, leading to self-excited oscillation of the bridge deck and the flutter instability takes place.

Fig. 10 shows the instantaneous pressure contours around the Second Forth Road Bridge deck during a typical cycle of the rotational oscillation. In snapshots (a), the flow is separated at the leading sharp corners in the upper and lower surface of the bridge deck. From snapshot (b) to (c), on the upper surface, the separated shear layer at the leading edge is enhanced by the rotational oscillation of the bridge deck, leading to an increase in the size of the negative pressure region. In this process, the

separated shear layer at the leading edge on the lower surface is very small and little changed. The first three snapshots correspond to the creation of the separation vortex on the upper surface. From snapshot (c) to (e), the vortex travels downstream along the upper surface of the bridge deck. In this process, as the rotational amplitude becomes small, accordingly, the negative pressure region in the leeward becomes smaller. In snapshot (f) the separation vortex drifts to the wake and the flow is completely separated from the lower surface of the bridge deck. From snapshot (f) to (h), the negative pressure region on the lower surface becomes smaller and smaller and changes into positive in the leeward region. At the same time, on the upper surface, the size of the negative pressure region in the leeward is increasing with time, and in the end the upper surface is fully covered by the negative pressure. In succession, the next cycle restarts. In Fig. 10, the separation and attachment points of the shear separated layer can be found to oscillate forward and backward along the body surface as the bridge deck oscillates, which leads to pressure fluctuations. This phenomenon is responsible for the increase in the amplitudes of the structural response observed in Figs. 8 (d) and 9 (d).

Table 2. Comparison of the flutter onset velocity of the Second Forth Road Bridge

Source	Critical velocity (m/s)
The present result	80.05
Numerical result [2]	77.5
Experimental result [2]	79.248 ± 7.488

Table 2 presents a comparison between the flutter onset velocity obtained by the present numerical simulation and the previously obtained numerical result and the experimental result [2]. It can be recognized that the present numerical result is reasonably in good agreement with the experimental data and the numerical value evaluated from aerodynamic derivatives.

3.2 Flutter analysis of the Guamá River Bridge

The flutter behavior of the Guamá River Bridge is studied as the second case to validate the present method. It has been previously studied by Rocha and Souza [30] in wind tunnel tests. The

geometrical features of the bridge deck are shown in Fig. 11 [5, 30]. All the simulations are performed at the Reynolds number (considering B=14.2 m as the characteristic dimension) Re= 2×10^5 , which is consistent with the Reynolds number in wind tunnel tests [30].
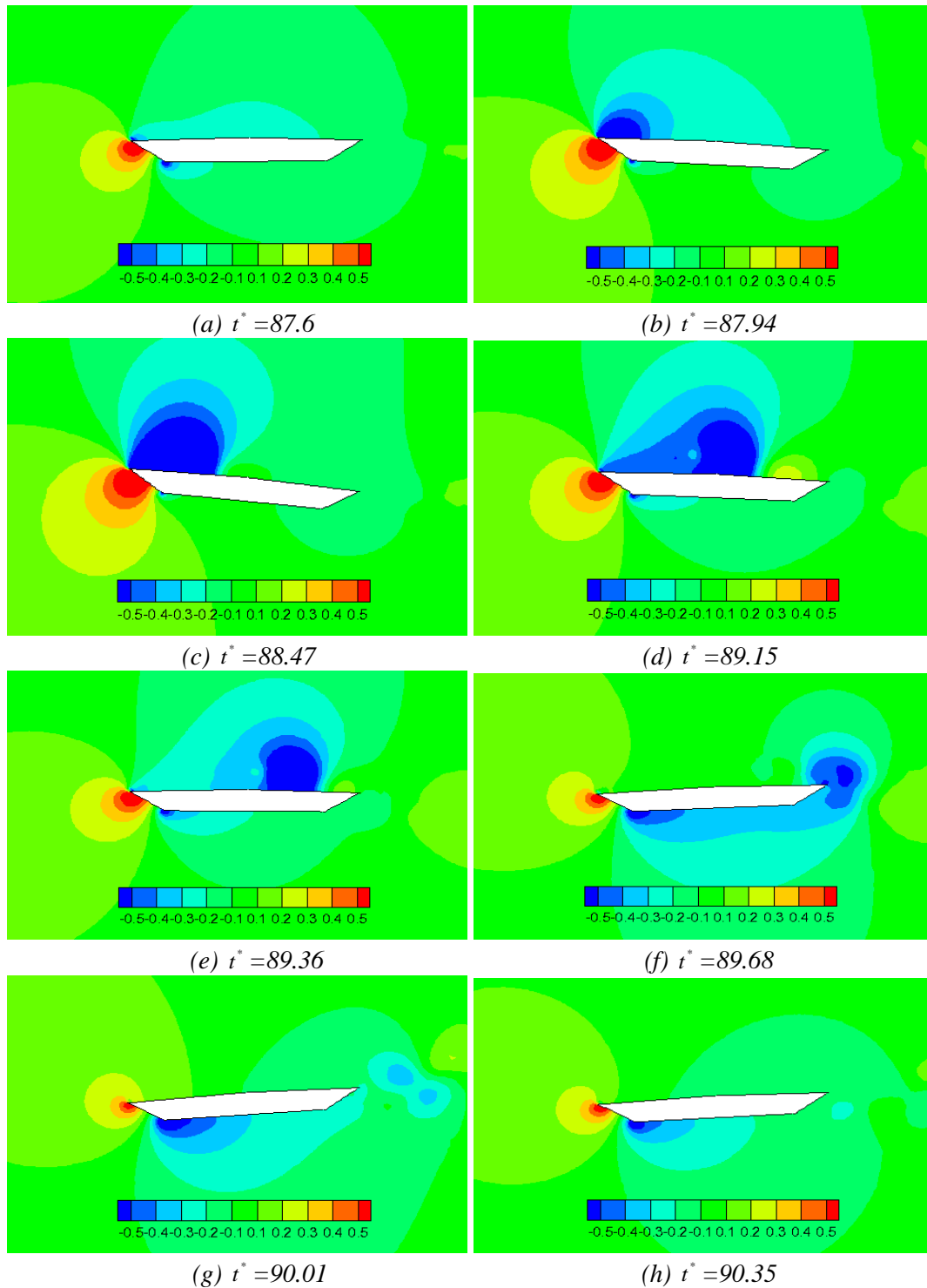

Figure 10. Instantaneous pressure contours around the Second Forth Road Bridge deck at eight chosen instants during one cycle of the rotational oscillation, U=81 m/s.

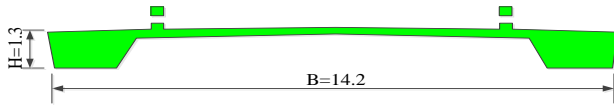The mechanical properties of the structure used in this paper are summarized in Table 3 [5, 30].

Figure 11. Geometrical characteristics of Guamá River Bridge.

Table 3. Mechanical properties of the structure

Characteristics	Value
Overall Width (B)	14.2 m
Mass per unit length	22513 kg/m
Mass moment of inertia	566838 kgm^2/m
Vertical natural frequency	0.331 Hz
Angular natural frequency	0.649 Hz
Damping ratio	0.3%

The arrangement of the computational domain is shown in Fig. 12. The elastic centre of the bridge deck is 5B away from the inlet while it is located 5B far from the upper and lower boundaries in our simulation. In this case, three grid sizes are used with the coarse-to-medium lattice spacing ratio m=4 and the medium-to-fine lattice spacing ratio m=4. As illustrated in Fig. 12, the fine-mesh block with lattice of 400×800 covers the area from 4.5B to 6.5B on x-axis and 4.5B to 5.5B on y-axis. The medium-mesh block covers the area from 4B to 8B on x-axis and 4B to 6B on y-axis. There are 320000 fine grids, 60000 medium grids, and 101250 coarse grids with a total of about 481250 grids in the entire domain. The boundary conditions for the simulations are the same as that for the flow past the Second Forth Road Bridge.

In wind tunnel tests, the critical velocity for the onset of flutter instability is evaluated from a critical value of the structural response, and a RMS (root mean square) angular displacement equal to 0.5° is taken as the critical displacement pattern. This RMS value corresponds to a peak angular displacement of 1.5°. Thus the peak angular displacement of the bridge deck that is equal to 1.5° is defined as the critical condition for the onset of flutter instability in the present work.
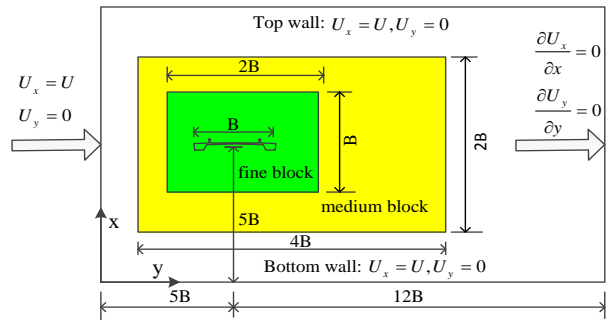

Figure 12. Flow geometry, computational domain and boundary conditions.

The flutter instability of the Guamá River Bridge is investigated by analyzing its structural response under wind action with four different wind velocity levels: 50, 56, 56.2 and 57. Initially, the bridge deck remains fixed with zero angle of attack. After 10000 time steps, the fluid force acting on the body surface has been computed, and then, the bridge deck is allowed to oscillate freely in the wind fields.

Fig. 13 displays the rotational displacement time histories of the bridge for the different velocities. The maximum amplitudes of the rotational displacement are determined and they are labelled in Fig. 13 as a black square. It can be seen from this Fig. that, the maximum amplitudes of the rotational displacement rise by increasing the inflow velocity At U=50 m/s and U=56 m/s, the maximum magnitudes of the oscillations are less than 1.5°. It suggests that at these two wind velocity levels, the flutter phenomenon has not occurred yet. At U=56.2 m/s, the maximum magnitude of the oscillations is just larger than 1.5°. It indicates that U=56.2 m/s is the critical velocity for the onset of flutter instability. The experiment shows the onset velocity of flutter instability at U=55 m/s [27]. Thus, the present simulations successfully simulated the critical velocity for the onset of flutter instability.

Fig. 14 illustrates the instantaneous pressure contours around Guamá River Bridge deck during one cycle of the rotational oscillation. As shown in this figure, the pressure distribution around Guamá River Bridge deck clearly shows the transient effect of the flow that is caused by the motion of the bridge deck.
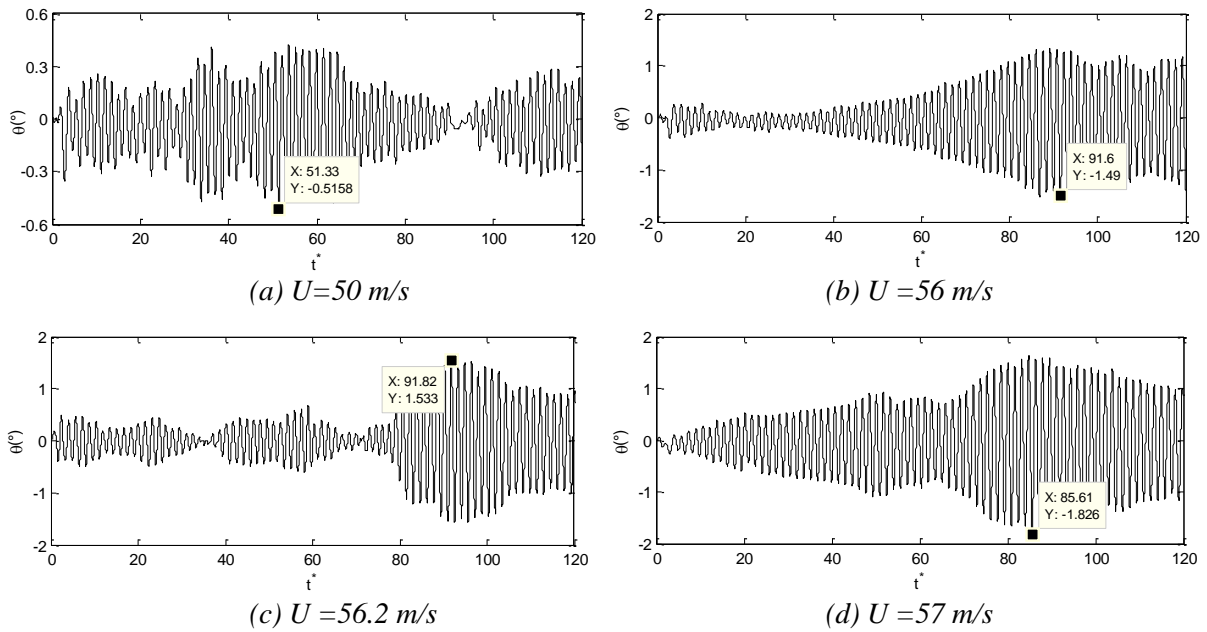
(a) U=50 m/s

(b) U =56 m/s

(c) U =56.2 m/s

(d) U =57 m/s

Figure 13. Rotational displacement of Guamá River Bridge.

(a) t =91.03*
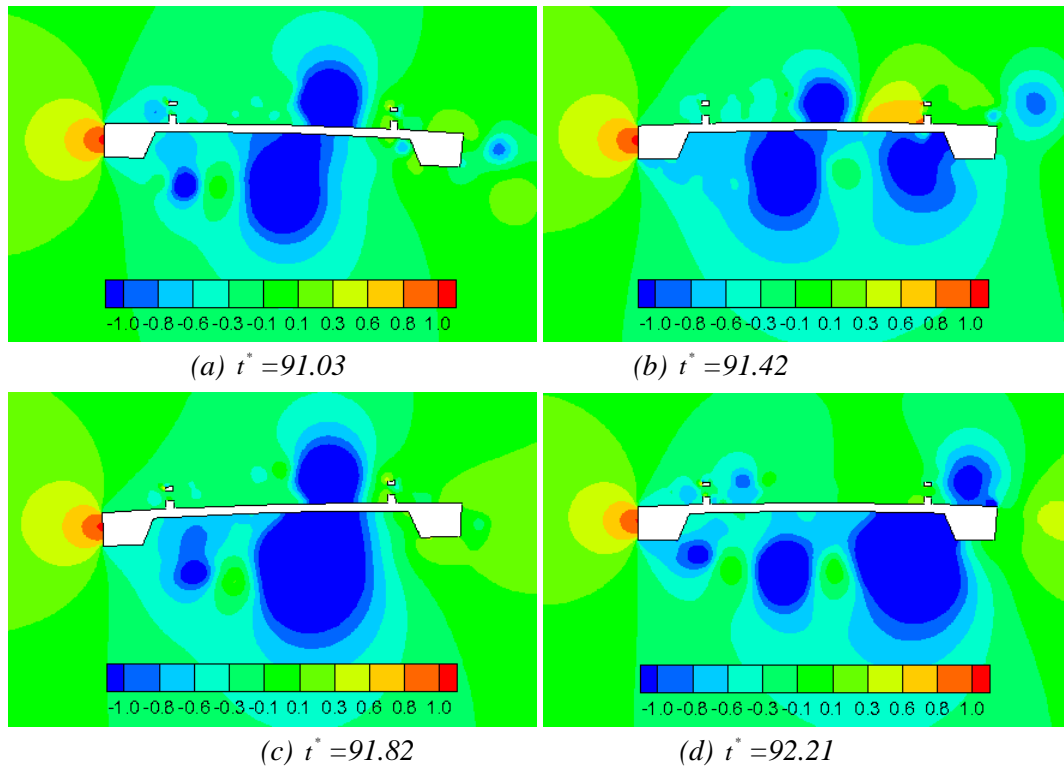
(b) t =91.42*

(c) t =91.82*

(d) t =92.21*

Figure 14. Instantaneous pressure contours around Guamá River Bridge deck at four chosen instants during one cycle of the rotational oscillation, U=56.2 m/s.

___

4. Conclusion

This paper presents a staggered coupling algorithm for fluid–structure interaction analysis of incompressible flows and rigid structures. In this algorithm, the unsteady fluid field is solved by two-dimensional multiple - relaxation - time Lattice Boltzmann Method with dynamic Smagorinsky subgrid scale model, while the rigid-body dynamic equation is solved by a Runge–Kutta method. Flutter analysis of the Second Forth Road Bridge and the Guamá River Bridge are performed by means of the presented computational algorithm.

The results show that the flutter onset velocities of the Forth Road Bridge and the Guamá River Bridge are in good agreement with both experimental and other existing numerical results. In this sense, the presented algorithm is suitable for providing reliable results needed for flutter analysis and is expected to be a quite suitable method for dealing with the wind-structure interaction problems, such as vortex-induced vibrations and galloping of civil engineering structures.

Acknowledgments

References

[1] Štimac Grandić, I., Ivančić, A., Liker, B.: *Parametric analysis of wind action on slab bridge deck*, Engineering Review, 31 (2011), 1, 45-54.

[2] Robertson, I., Sherwin, S. J., Bearman, P.W.: *Flutter instability prediction techniques for bridge deck sections*, International Journal for Numerical Methods in Fluids, 43 (2003), 10-11, 1239–1256.

[3] Frandsen, J.B.: *Numerical bridge deck studies using finite elements. Part I: flutter*, Journal of Fluids and Structures, 19 (2004), 2, 171–191.

[4] Badia, S., Codina, R.: *On some fluid–structure iterative algorithms using pressure segregation methods. Application to aeroelasticity*, International Journal for Numerical Methods in Engineering, 72 (2007), 1, 46–71.

[5] Braun, A. L., Awruch, A. M.: *Finite element simulation of the wind action over bridge sectional models: Application to the Guamá River Bridge (Pará State, Brazil)*, Finite Elements in Analysis and Design, 44 (2008), 3, 105-122.

[6] Sarkic, A., Fisch , R., Hoffer, R., Bletzinger, K.U.: *Bridge flutter derivatives based on computed, validated pressure fields*, Journal of Wind Engineering and Industrial Aerodynamics, 104-106 (2012), 141-151.

[7] De Miranda, S., Patruno, L., Ubertini, F., Vairo, G.: *Indicial functions and flutter derivatives: A generalized approach to the motion-related wind loads*, Journal of Fluids and Structures, 42 (2013), 466-487.

[8] Brusiani,F., de Miranda, Patruno, L., Ubertini, F., Vaona, P.: *On the evaluation of bridge deck flutter derivatives using RANS turbulence models*, Journal of Wind Engineering and Industrial Aerodynamics, 119 (2013), 39-47.

[9] Farsani, H. Y., Valentine, D. T., Arena, A., Lacarbonara, W., Marzocca, P.: *Indicial functions in the aeroelasticity of bridge decks*, Journal of Fluids and Structures, 48 (2014), 203 -215.

[10] Selvam, R. P., Tarini, M. J., Larsen, A.: *Computer modelling of flow around bridges using LES and FEM*, Journal of Wind Engineering and Industrial Aerodynamics, 77-78 (1998), 1, 643-651.

[11] Patro, S. K., Selvam, R. P., Bosch, H.: *Adaptive h-finite element modeling of wind flow around bridges*, Engineering Structures, 48 (2013), 569–577.

[12] Sarwar, M.W., Ishihara, T., Shimada, K., Yamasaki, Y., Ikeda, T.: *Prediction of aerodynamic characteristics of a box girder bridge section using the LES turbulence model*, Journal of Wind Engineering and Industrial Aerodynamics, 96 (2008), 10-11, 1895-1911.

[13] Mannini, C., Šoda, A., Voß, R., Schewe, G. : *Unsteady RANS simulations of flow around a bridge section*, Journal of Wind Engineering and Industrial Aerodynamics, 98 (2010), 12, 742-753.

[14] Succi, S.: The Lattice-Boltzmann Equation: For Fluid Dynamics and Beyond. Oxford University Press, Oxford, 2001.

[15] Benzi, R., Succi, S., Vergassola, M.: The lattice Boltzmann equation: theory and applications. Physics Reports. 222 (1992), 3, 145–197.

_____

[16] Garcia, M., Gutierrez, J., Rueda, N.: *Fluid–structure coupling using lattice-Boltzmann and fixed-grid FEM*, Finite Elements in Analysis and Design, 47 (2011), 8, 906-912.

[17] De Rosis, A., Falcucci, G., Ubertini, S., Ubertini, F., Succi, S.: *Lattice Boltzmann analysis of fluid–structure interaction with moving boundaries.* Communications in Computational Physics, 13 (2012), 3, 823-834.

[18] De Rosis, A., Falcucci, G., Ubertini, S., Ubertini, F.: *Aeroelastic study of flexible flapping wings by a coupled lattice Boltzmann-finite element approach with immersed boundary method*, Journal of Fluids and Structures, 49 (2014), 516-533.

[19] Meldi, M., Vergnault, E., Sagaut, P.: *An arbitrary Lagrangian–Eulerian approach for the simulation of immersed moving solids with Lattice Boltzmann Method*, Journal of Computational Physics, 235 (2013), 15, 182-198.

[20] d'Humieres, D.: *Generalized lattice-Boltzmann equations, in rarefied gas dynamics: theory and simulations,* Progress in Astronautics and Aeronautics, 159 (1992), 450–458.

[21] Yu ,D. Z., Mei, R. W., Luo, L. S., Shyy, W.: *Viscous flow computations with the method of lattice Boltzmann equation*, Progress in Aerospace Sciences, 39 (2003), 5, 329-367.

[22] Bhatnagar, P. L., Gross, E. P., Krook, M.: *A model for collision processes in gases. I. Small amplitude processes in charged neutral one-component systems*, Physical Review, 94 (1954), 511–525.

[23] Lallemand, P., Luo, L.S.: *Theory of the lattice Boltzmann method: dispersion, dissipation, isotropy, Galilean invariance, and stability*, Physical Review E, 61 (2000), 6546–6562.

[24] Germano, M., Piomelli, U., Moin, P., Cabot, W.: *A dynamic subgrid-scale Eddy viscosity model*, Physics of Fluids A, 3 (1990), 7, 1760.

[25] Premnath, K. N., Pattison, M. J., Banerjee, S.: *Dynamic subgrid scale modeling of turbulent flows using lattice-Boltzmann method*, Physica A , 388 (2009), 2640-2658.

[26] Filippova, O., Hänel, D.: Lattice Boltzmann simulation of gas-particle flow in filters. Computers & Fluids, 26 (1997), 7, 697-712.

[27] Caiazzo, A.: Analysis of lattice Boltzmann nodes initialisation in moving boundary problems, Progress in Computational Fluid Dynamics, an International Journal, 8 (2008), 1-4, 3-10.

[28] Caiazzo, A.: Analysis of lattice Boltzmann initialization routines, Journal of statistical physics, 121 (2005), 1-2, 37-48.

[29] Yu, D. Z., Mei, R.W., Shyy, W.: *A multi-block lattice Boltzmann method for viscous fluid flows*, International Journal for Numerical Methods in Fluids, 39 (2002), 2, 99–120.

[30] Rocha, M. M., Loredo-Souza, A. M., Nuñez, G.J.Z.: *Experimental analysis of the aerodynamic stability of the Guamá River Bridge*, Proceedings of the 30th South-American Journey on Structural Engineering, Brasília (DF), Brasil, 2002.